

압출 3D 프린팅에서 에폭시 복합재료의 유변학적 및 프린팅 거동

Jianzhong Shang[†], Xin Li, Rong Wang, and Zhuo Wang

College of Mechatronics Engineering and Automation, National University of Defense Technology
(2017년 4월 14일 접수, 2017년 5월 11일 수정, 2017년 5월 24일 채택)

Rheological and Printable Behavior of Epoxy Resin-based Materials for Extrusion 3D Printing Applications

Jianzhong Shang[†], Xin Li, Rong Wang, and Zhuo Wang

College of Mechatronics Engineering and Automation, National University of Defense Technology,
Changsha 410073, P.R. China

(Received April 14, 2017; Revised May 11, 2017; Accepted May 24, 2017)

Abstract: This study investigates rheological and extrusion behavior of thermosetting epoxy resins. The purpose is to find the universal property and printing parameters for extrusion based rapid prototyping applications. The thickener proportion greatly influences its viscosity and rheological behavior and therefore plays an important role in the shape of the cross-section of the extrudate. In addition to the effects of the rheological behavior of the composite, shape maintenance and its wettability on the substrate, the cross-sectional geometry of the extrudate is also strongly affected by printing process parameters including the extrusion nozzle height, nozzle moving speed, extrusion rate, and critical nozzle height. Proper combinations of these process parameters are necessary in order to obtain single line extrudates with plump cross-sections and 3D objects with dimensional accuracy, uniform wall thickness, good wall uprightness, and no wall slumping. Formulas and procedures for determining these extrusion parameters are proposed and demonstrated in experiments.

Keywords: epoxy resins, rheological behavior, printable behavior, 3D printing, extrusion parameters.

Introduction

Direct extrusion fabrication (DEF), a new branch of solid freeform fabrication (SFF),¹ is an automated fabricating process that builds 3D complex-shaped structures layer-by-layer directly from CAD files without part-specific tooling, heating and human intervention. The development in DEF has offered opportunities to manufacture complex-geometry components and systems with highly integrated and multi-functions that could not be easily fabricated using conventional approaches.²⁻¹¹ With the rapid development of new materials, the advantage of DEF is increasingly obvious day by day. Theoretically, DEF could use any pasty and gel-like composite material with additions, which don't change its shape maintenance to fabricate.

Thermosetting epoxy resin based composites have been widely used in many fields because of its good mechanical

properties and chemical stability. At present, it is a trend that more and more metal structures have been replaced by polymer. These materials exhibit Young's modulus values that are an order of magnitude higher than those obtained by thermoplastics and photocurable resins developed for commercial 3D printing methods, while retaining comparable strength.

One of the key issues in the DEF process is to extrude materials to the desired location precisely with controlled shape. In the case of routing lines, rectangular cross-section with a 90° contact angle is desired so that voids between the lines routed can be prevented or minimized. Furthermore, the routed pastes lines should be sufficiently fine (ranging from 0.2 to 1.0 mm). And one of the most basic requirements of the composites materials is shape maintenance, which can be satisfied by proper rheological behavior.¹²⁻¹⁴

Currently, there are two general methods for preparing the epoxy based composites (EBC) for DEF. One is to prepare aqueous EBC without addition of binders and to control the cross-sectional geometry of the extrudate by adjusting the pH value, salt concentration, and volume fraction of solid in the

[†]To whom correspondence should be addressed.

E-mail: jz_shang_nudt@yeah.net

©2017 The Polymer Society of Korea. All rights reserved.

epoxy.^{3,17-20} The second method requires the use of polymers or resins as the binder in order to maintain the shape of the extrudate.^{15,16} Using fine Al_2O_3 powder, Cesarano *et al.*¹⁷ have shown that when an EBC is pseudoplastic and drying rates are appropriate, the lines extruded yield nearly rectangular cross-sections with relatively straight walls and flattened tops. The EBC formulation and particle size have also been shown by Du *et al.*²¹ to have strong effects on the extrudability of thin wall tubes and their thickness and uniformity.

Although the effects of rheological behavior of the EBC on the cross-sectional geometry of the extrudate have been studied by several researchers,^{3,17-20} the dependency of the shape maintenance and rheology behavior on materials preparation and extrusion parameters has not been systematically investigated. This is especially the case for micro-extrusion with the line width of the extrudate <1 mm. To address this issue, the effects of extrusion parameters on the cross-sectional geometry of the extrudate in conjunction with the effects of rheological behavior of EBC have been investigated in this study. Such a study is of not only scientific interest but also technological importance because nozzles with an opening smaller than 1 mm are normally circular in shape and it is important to find out how to achieve extrudates with a near-rectangular cross-section using circular nozzles. In this study, alginate with EBC binders are used because the EBC without addition of binders are not desirable in order to satisfy the requirement of the forming of EBC. The extrusion parameters investigated include the nozzle height of the extruder, nozzle moving speed, extrusion rate, and critical nozzle height. The rheology behavior of materials contains shear yield strength, storage modulus, loss modulus. These parameters have been investigated because all of them are experimental variables and can be adjusted independently to achieve the desired.

Experimental

We first prepared the EBC that embody the essential rheological properties required for our 3D printing method. Unlike prior printing material designs that undergo solidification via gelation, drying, or on-the-fly photopolymerization,²¹⁻²⁴ epoxy resins are reactive materials that initially exhibit a low viscosity, which rises over time as the reaction proceeds under ambient conditions. Moreover, these EBC ultimately require thermal curing at elevated temperatures (100-220 °C) for several hours to complete the polymerization process. We developed epoxy-based EBC that exhibited the desired vis-

coelasticity and long pot-life in the absence and presence of highly anisotropic fillers. Specifically, we formulated the base epoxy EBC using an epoxy resin (Epon 826 epoxy resin, Jiaweida Biotechnology Inc.) with appropriate amounts of dimethyl methyl phosphonate (DMMP, Sigma Aldrich, St. Louis, MO), alginates powders (Jiaweida Biotechnology Inc., 100 nm dominant), using a Thinky Planetary Centrifugal Mixer (Thinky USA, Inc., Laguna Hills, CA) in a 125 mL glass container using a custom adaptor. An imidazole-based ionic liquid is employed as a latent curing agent (Basionics VS03, BASF Intermediates, Ludwigshafen, Germany). The alginates primarily serve as a rheology modifier that imparts both shear thinning behavior and a shear yield stress to the uncured EBC, while DMMP serves to reduce the initial viscosity of the resin to allow higher solids loading. Both of these additives may also enhance the mechanical properties of the cured epoxy matrix.^{25,26}

The EBC batches started with 30 g of Epon 826 resin. 3 g of DMMP are added, followed by 10 min of mixing in the Thinky mixer. Next, alginates were added in 22.5 g increments. After adding each constituent to the EBC, it is mixed for 13-15 min in the Thinky mixer. Finally, the EBC was allowed to cool to room temperature prior to the addition of the curing agent, Basionics VS03, at 5 wt% of the total epoxy resin added. After the addition of the curing agent, the EBC was mixed for additional 13 min.

The EBC were loaded into a 50 mL-extruder and centrifuged at 3600 rpm for 10 min to remove bubbles. Loaded extruder was then mounted in a turbine worm drive reducer (reduction ratio of 7.25:1), which was placed on an extrusion type 3D printer (designed and constructed at the National University of Defense Technology). The EBC was driven electrically and controlled via a planetary reduction step motor and TB6600 controller (Yixing Inc.). The EBC was extruded onto the temperature auto-controlled platform with a nozzle of circular shape 800 μm in diameter. Print paths for each geometry was written as parameterized g-code scripts and designed to maximize continuity within each printed layer. Printed parts were pre-cured at 100 °C for 15 h, cooled, removed from the substrate, and cured for 2 h at 220 °C.

The EBC was extruded using an extrusion type 3D printer designed and constructed at the National University of Defense Technology. The machine consists of three major components: (i) the reducer that have a reduction ratio of 7.25:1, (ii) The turbine worm drive micro-extruders for EBC, (iii) an X-Y-Z positioning system. The pressure exerted on the EBC within the

micro-extruder was applied via motor with a nozzle of circular shape 800 μm in diameter. The motion and position control were provided by a computer through a Galil DMC-1800 multi-axis motion control card. Rheological properties of the EBC were characterized using a HAAKE MARS III rheometer (TA Instruments, New Castle, DE) with a pp25 flat plate geometry and a gap of 500 μm for the EBC with different proportion of alginates. The cross-section geometry was evaluated by the line width and height of the extrudate and its contact angle with the substrate. To measure these geometrical parameters, the lines extruded were encapsulated using pure epoxy before cutting and polishing after which these parameters were observed and measured using an optical microscope.

Results and Discussion

Rheological Behavior of EBC. The rheological behaviors of EBC of varying composition are shown in Figure 1 and Figure 2. The pure epoxy exhibits a viscosity (η) of $\sim 2 \text{ Pa}\cdot\text{s}$ that is independent of shear rate (Figure 1). As a consequence, the shear storage modulus (G') of this base epoxy is lower than its loss modulus (G''), and both moduli are independent of applied shear stress (Figure 2). While the base epoxy readily flows through nozzles under modest pressures, it immediately wets and spreads upon exiting the nozzle and lacks the ability to support itself. The addition of alginate transforms the epoxy into a viscoelastic fluid. The resulting material, referred to as the EBC (30 wt% alginate), possesses a η that close to $10^5 \text{ Pa}\cdot\text{s}$ at low shear rates ($\sim 0.01 \text{ s}^{-1}$) that is five orders of magnitude higher than the base epoxy. Due to its shear thinning behavior, this EBC exhibits an apparent viscosity of $\sim 10^3 \text{ Pa}\cdot\text{s}$ at shear rates ($\sim 50 \text{ s}^{-1}$) typically experienced during printing. Hence, the EBC viscosity is only less than three orders of magnitude higher than that of the epoxy alone under relevant printing conditions. The EBC (10 wt% alginate) exhibits a plateau value of $G' \sim 321 \text{ Pa}$ that exceeds G'' by about 80 Pa at low stress. At the crossover point between the two moduli curves, its shear yield stress (τ_y) is $\sim 3.2 \text{ Pa}$. Upon adding 20 wt% alginate to the base epoxy, the viscosity increases to more than double magnitude at a given shear rate without altering its shear thinning behavior. At the characteristic shear rate of 50 s^{-1} , the viscosity of the EBC (20 wt% alginate) is $\sim 70 \text{ Pa}\cdot\text{s}$. And the EBC (20 wt% alginate) exhibits a plateau value of $G' \sim 2021 \text{ Pa}$ that is more than twice as large as G'' at low stress. At the crossover point between the two moduli curves, its shear yield stress (τ_y)

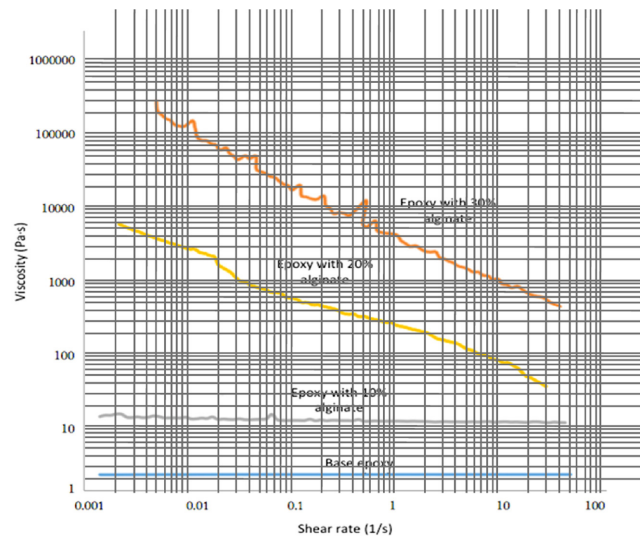


Figure 1. Plot of viscosity as a function of shear rate.

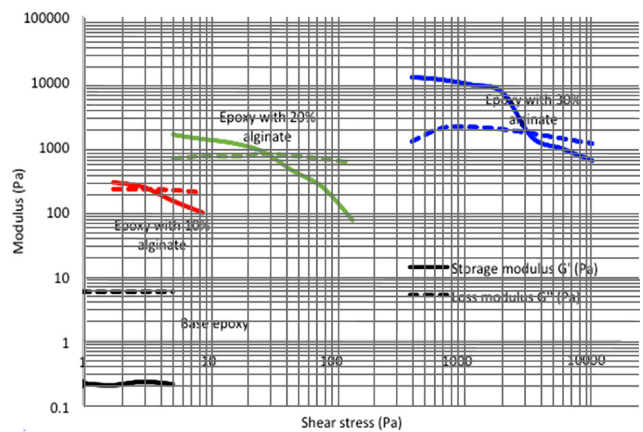


Figure 2. Log-log plot of shear storage and loss moduli as a function of shear stress for epoxy-based materials of varying composition.

is $\sim 34 \text{ Pa}$. Then, adding 30 wt% alginate to the base epoxy, at the shear rate of 50 s^{-1} , the viscosity is $\sim 914 \text{ Pa}\cdot\text{s}$, the EBC (30 wt% alginate) exhibits a plateau value of $G' \sim 10244 \text{ Pa}$ that exceeds G'' by about one order of magnitude at low stress. At the crossover point between the two moduli curves, its shear yield stress (τ_y) is $\sim 3017 \text{ Pa}$.

Finally, the addition of more than 30 wt% alginate to the base epoxy has little effect on either the viscosity or degree of shear thinning. Due to their high stiffness and yield stress, these materials are ideally suited for 3D printing of cellular composites. Figure 3 compares the contact angle of the extrudates with the addition of alginate values equal to 10, 20, and 30 wt%. At 10 wt%, the EBC is very stable with a low viscosity. As a result, the EBC flows continuously after it leaves

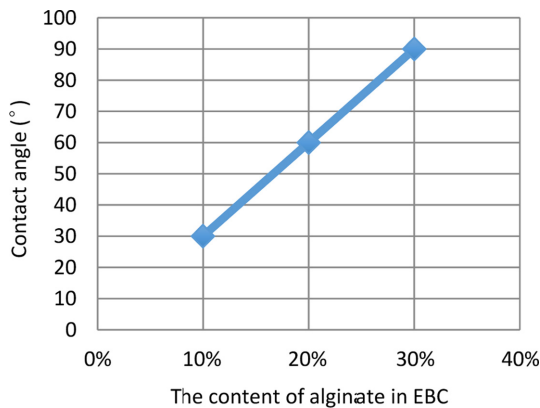


Figure 3. Contact angle of EBC with different mass fraction of alginate.



Mass fraction of alginate	10%	20%	30%
Contact angle	30°	60°	90°

Figure 4. Cross-sectional photos of extrudates with different mass fraction of alginate.

the nozzle and thus takes on an arch shape with a low contact angle of 30°. At 20 wt%, the viscosity of the EBC increases and thus the EBC spreads out less on the surface of the substrate, resulting in an increased contact angle of 60°. At 30 wt%, the EBC becomes pseudoplastic. As a result, the contact angle of the extrudate with the substrate increases to 90°, clearly indicating nearly no spreading after the EBC leaves the nozzle of the extruder.

Figure 4 compares the cross-sectional geometry of the extrudates with mass fraction of alginate equal to 10, 20, and 30 wt%. With a contact angle near 90°, the cross-section of the extrudate is approaching a rectangular shape which is highly suitable for fabrication of 3D objects through layer-by-layer approaches.

Effects of the Nozzle Height on the Cross-sectional Geometry of Extrudates. The nozzle height, which is defined as the distance between the nozzle tip of the extruder and the substrate, greatly influences the cross-sectional geometry of the extrudate. The distance between the nozzle and the substrate will limit the space within which the EBC can flow. For a given set of the extrusion rate, nozzle diameter and nozzle moving speed, there is an optimal nozzle height (h_o , mm). When the nozzle height is smaller than h_o , the volume of EBC extruded will be too large for the space between the nozzle and the substrate. As a result, the EBC is forced to spread in the

directions perpendicular to the deposited line, and the resultant shape of the extrudate is not only determined by the rheological properties and wettability of the EBC, but also by the nozzle height. In contrast, when the nozzle height is larger than h_o , there is enough space for the deposited EBC so that the cross-sectional geometry of the extrudate is only dictated by the rheological properties and wettability of the EBC. However, in the process of 3D printing, large nozzle height will reduce the accuracy of printing. When the printing paths are circular arcs, the radius of deposited path will be smaller than that of the nozzle path, which is called arc effect. Our experiments indicate that the critical nozzle height can be estimated using the following eq. (1):

$$h_o = \alpha \frac{V_e}{D_n v_n} \quad (1)$$

where, V_e is the volume of the EBC extruded per unit time (called the extrusion rate, mm³/s), D_n is the nozzle diameter (mm), and v_n is the nozzle moving speed with respect to the substrate (mm/s). α is a proportional coefficient ($0 < \alpha < 1$), which is related to the EBC's rheological characteristics. The physical meaning of eq. (1) is that the volume of the EBC extruded per unit time is equal to the volume available per unit time between the nozzle and the substrate (considering rheological behavior of EBC, α is introduced to revise the model). When the nozzle height is lower than h_o , there will be a squeezing effect, i.e., the EBC is forced to take up the space beyond the volume defined by the product of the nozzle height, the nozzle diameter, and the distance traveled by the nozzle per unit time. Finally, it should be noted that V_e , v_n and D_n are all experimental variables and can be varied independently. Thus, a particular h_o can be obtained by a combination of different V_e , v_n and D_n .

Figure 5 shows the contact angle of the extrudate with same rheological characteristics as a function of the nozzle height. When the nozzle height equals to 150 and 300 μ m, the EBC spread widely along the substrate with low contact angles. When the nozzle height equals to 745 μ m, the contact angle closes to 90° and no spreading is observed. Therefore, $\alpha=0.82$ can be obtained by experiment. A further increase in the nozzle height (800 μ m) does not alter the shape of the extrudate much with only a small increase in the contact angle. The critical nozzle height calculated using eq. (1) for the extrusion condition shown in Figure 5 is 750 μ m, which is between 480 and 800 μ m tested in the experiment. These results indicate that when the nozzle height is near the critical nozzle height, the

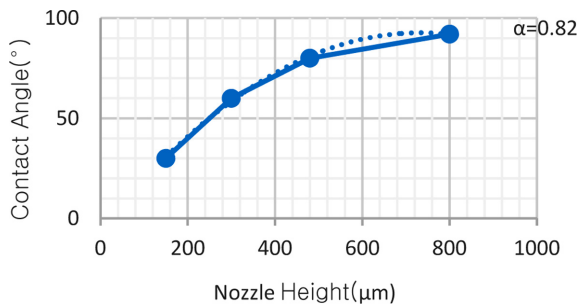


Figure 5. Contact angle as a function of the nozzle height for the EBC with 30 wt% alginate. Other extrusion parameters are $V_c=4$ mm³/s, $D_n=0.8$ mm, and $v_n=5.5$ mm/s.

contact angle of the EBC on the substrate used in this study is about 90°. However, when the nozzle height is substantially smaller than h_o (e.g., the cases of 150 and 300 μm in Figure 5), the forced flow is occurred and the contact angles will be smaller than 90°.

Influence of the Shear Rate on the Cross-sectional Geometry of Extrudates. Because of the pseudoplastic behavior of the EBC, extrusion conducted with high shear rates will have relative low viscosity, whereas extrusion with low shear rates will have high viscosity. When the EBC contacts the substrate after leaving the nozzle, the shear rate decreases to zero. This will lead to the highest viscosity of the EBC, which in turn will hinder the flow of the EBC and freeze the extrudate. Thus, the viscosity difference between the EBC leaving the nozzle and the EBC contacting the substrate will affect how fast the EBC can spread along the surface of the substrate, and thus influence the cross-sectional geometry of the extrudate. In order to precisely investigate the effect of the shear rate, the experiments have been designed in which both the extrusion rate and the nozzle moving speed have been increased proportionally, so that the critical nozzle height are kept constant (see eq. (2)). Thus, only the effect of the shear rate is evaluated because the nozzle height and the critical nozzle height are kept constant.

The results from this special set of the experiments are shown in Figure 6. At high shear rates (50 and 100 s⁻¹), the contact angles are smaller than 90°. In contrast, at low shear rates (10 and 25 s⁻¹), contact angles are greater than 90°. This is so because high shear rates lead to low viscosities (see Figure 7), and thus the EBC flows fast after it leaves the nozzle tip. As a result, the EBC spreads along the surface of the substrate before it freezes and a low contact angle results. In contrast, when low shear rates are used, the flow of the EBC after it leaves the nozzle tip is limited because of its high viscosity.

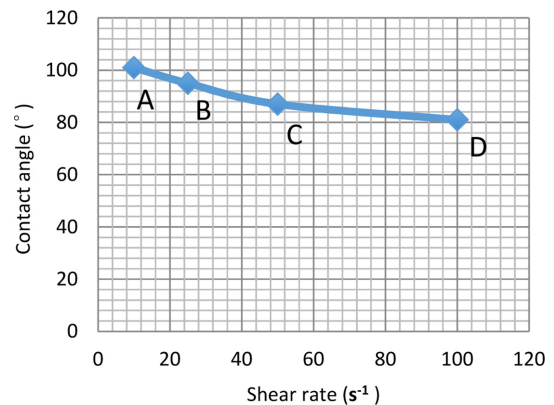


Figure 6. Contact angle as a function of the shear rate (achieved by changing the extrusion rate and the nozzle moving speed proportionally) while keeping all other processing parameters constant. The extrusion rate (mm³/s) and the nozzle moving speed (mm/s) are 10.0 and 11.5 for point D, 5.0 and 5.8 for point C, 2.5 and 2.9 for point B, and 1.0 and 1.2 for point A.

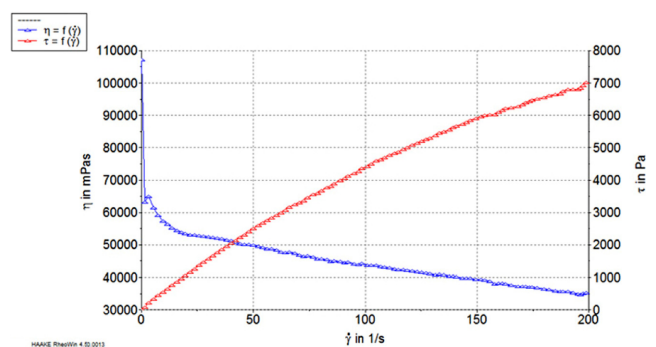


Figure 7. Viscosity curve of EBC (30 wt% alginate) from the shear rate of 10⁻² to 200 s⁻¹.

As a consequence of this limited flow, a high contact angle forms. It is noted, however, that in spite of the dependency of the cross-sectional geometry on the shear rate, the effect of the shear rate on the contact angle is relatively small in comparison with that of the nozzle height. As seen from Figure 6, the variation of the contact angle due to different shear rates investigated is within 20 wt%, which is much smaller than 67.4% changes achieved by altering the nozzle height (Figure 5).

As it can be seen in Figure 1, the viscosity of EBC decreased as the shear rate increased. And the start point of the experiments is 0.002 s⁻¹, which is nearly equal to zero. However, in Figure 6, the contact angle is nearly 100° when the shear rate is 10⁻¹. During the experiments, we found that under the condition of 0~10 s⁻¹, the EBC is almost pasty, that means the contact angle will be all larger than 90° when the shear rate is

smaller than 10 s^{-1} .

Influence of the Extrusion Rate and Pressure on the Cross-sectional Geometry of Extrudates. The cross-sectional geometry of extrudates is expected to be influenced by the extrusion rate and pressure. When the geometry and dimensions of extruder and the formulation of EBC are fixed, the extrusion pressure P and the EBC extrusion rate V_e , are directly related to each other via the following eq. (2)²⁷

$$P = 2 \left(\sigma_0 + \frac{4\beta V_e}{\pi D_n^2} \right) \ln \left(\frac{D_0}{D_n} \right) + 4 \left(\tau_0 + \frac{4\gamma V_e}{D_n^2} \right) \ln \left(\frac{L}{D_n} \right) \quad (2)$$

where, σ_0 is the yield stress of the EBC, τ_0 is the wall shear stress of the EBC at zero velocity, D_0 is the barrel diameter, L is the length of the nozzle, β and γ are factors that account for velocity dependence of the yield stress and wall shear stress of the EBC. It can be seen from eq. (2) that increasing the extrusion pressure increases the extrusion rate if all other parameters are kept constant. Thus, studies of the effect of the extrusion rate while keeping all other parameters constant are equivalent to the study of the effect of the extrusion pressure.

Figure 8 shows the effect of the extrusion rate on the cross-sectional geometry of extrudates. Keep three things in mind when interpreting the result of Figure 8. First, changing the extrusion rate also changes the flow rate of the EBC because the average flow rate of the EBC at the nozzle tip is equal to the extrusion rate divided by the nozzle diameter. Thus, at a constant nozzle diameter, increasing the extrusion rate increases the flow rate. Second, increasing the extrusion rate also alters the critical nozzle height (see eq. (1)). Thus, the result shown in Figure 8 should be considered as a combined

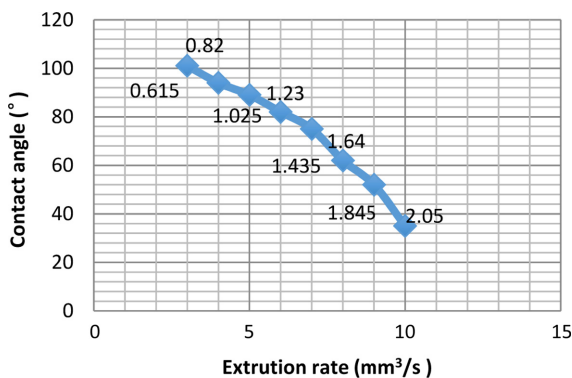


Figure 8. Contact angle as a function of the extrusion rate. Other extrusion parameters are $D_n = 0.8 \text{ mm}$, $h = 1 \text{ mm}$, and $v_n = 5 \text{ mm/s}$. The number shown with each point is the critical nozzle height used in the experiment.

effect of the shear rate and the critical nozzle height, rather than a simple shear-rate effect. Finally, given the relationship between the extrusion rate and extrusion pressure defined in eq. (2), the result in Figure 8 can also be interpreted as the effect of the extrusion pressure, which increases with the extrusion rate.

As seen from Figure 8, when the extrusion rate is high (e.g., $V_e = 9$ and $10 \text{ mm}^3/\text{s}$), the contact angle is smaller than 90° , which indicates that the EBC has spread along the substrate surface before it freezes. Such phenomenon is due to two factors: 1) the nozzle height (1 mm) is much lower than the critical nozzle heights (1.845 mm for $V_e = 9 \text{ mm}^3/\text{s}$ and 2.05 mm for $V_e = 10 \text{ mm}^3/\text{s}$), and 2) the high extrusion rates causes high shear rate, the viscosity of the EBC reduces. When the extrusion rate is intermediate (e.g., $V_e = 4$ and $5 \text{ mm}^3/\text{s}$), the contact angle becomes approximately 90° , which means little spreading of the EBC before it freezes. This is so because the forced flow is alleviated and the viscosity of the EBC is increased.

Optimization of Multi-layer Construction. The single line extrusion study described above has indicated that extruded lines with a near 90° -contact-angle cross-section can be obtained through proper control of the rheological behavior of the EBC, the nozzle height, the extrusion rate, the nozzle moving speed, and the critical nozzle height. However, the optimal conditions for extruding single lines may or may not be optimal for multiple layer construction. Thus, fabrication of multi-layered objects has been studied based on the understanding developed from the single line investigation. Furthermore, the study of fabrication of multi-layer objects is focused on the effect of the cross-sectional geometry of single lines on the dimensional accuracy, wall slumping, uniformity of wall thickness, wall uprightness, and shrinkage and dimensional stability during sintering. Thus, in order to minimize the number of experiments, the optimal values of the extrusion rate and the nozzle moving speed determined from the single line investigation have been adopted in the investigation of the multi-layer fabrication, whereas only the nozzle height is varied and investigated.

It is different from single line extrusion that due to the gravity effect, the critical nozzle height of multi-layer extrusion will be smaller. And the attenuation rate of the critical nozzle height is related to nozzle diameter (D_n). When objects are extruded with the nozzle height larger than the critical nozzle height, the objects produced contain distortion. The diameters of arcs parts vary with height although the computer models for both arcs parts have a constant diameter. This phenomenon

is related to the drag force exerted by the moving nozzle. Such a drag force is present under all extrusion conditions regardless of the nozzle height used. However, when the nozzle height is smaller than the critical nozzle height, the extrudate is forced to contact the previously deposited layer and bonds to it immediately. In contrast, when the nozzle height is larger than the critical nozzle height, the extrudate is dragged away before it contacts the previously deposited layer. In addition, the extrudate is lifted and dragged upwards during extrusion. Thus, when the nozzle is traveling along a circle, the extrudate bends towards the center of the circle owing to the drag force of the nozzle, leading to a circular extrudate with its diameter smaller than the diameter of the previously deposited layer (Figure 9(b)). Furthermore, the larger the nozzle height used, the more effective the drag force of the nozzle in bending and thus the smaller the extrudate diameter. The drag force of the nozzle, however, is balanced by the surface tension and the rigidity of the extrudate. In short, the shape and dimensions of the objects extruded with the nozzle height larger than the critical nozzle height cannot be predicted easily because of the strong influence of the nozzle drag force. In contrast, the dimensions of the objects extruded with the nozzle height equal to the critical nozzle height are predictable and match the computer models. The empirical equation of multi-layer extrusion critical nozzle height can be derived by experiments.

$$h_{cm} = \delta h_{cs} \cdot \frac{h_{cs}}{D_n} = \delta \cdot \frac{h_{cs}^2}{D_n} = \delta \cdot \alpha^2 \cdot \frac{V_e^2}{D_n^3 v_n^2} \quad (3)$$

Where, h_{cs} is the critical nozzle height of single layer, δ is the compensation factor. From eq. (3), it can be seen that if the extrusion rate and nozzle moving speed keep constant, h_{cm} is inversely proportional to the third power of D_n . It is noted that eq. (3) is based on the theoretical inference and test analysis, and it is suitable for the situation that the number of layers is less than 20 (the deviation reached 4.8%).

Figure 9 shows a six-layered single-wall object extruded with different nozzle heights at the same extrusion rate ($4 \text{ mm}^3/\text{s}$), nozzle diameter (0.8 mm), and nozzle moving speed (5.5 m/s). δ is 0.95 according to the rheological behavior of the EBC. The nozzle heights applied in fabricating the object are 0.65 mm and 0.75 mm, respectively. The critical nozzle height for fabricating both of the objects, however, is equal to 0.66 mm. Since the nozzle heights in Figure 9(b) is larger than the critical nozzle height, there is a nozzle dragging effect during extrusion. As a result, object in Figure 9(b) has a

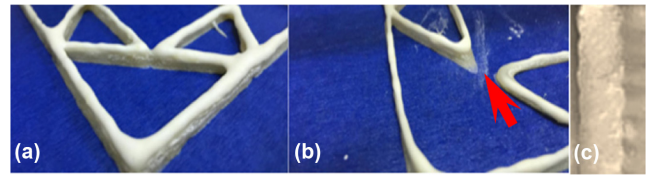


Figure 9. (a) The nozzle height is equal to the multi-layer critical nozzle height; (b) the nozzle height is larger than the multi-layer critical nozzle height, the diameter of the arcs is smaller than that of the previous layer; (c) the cross-sectional image of the multi-layer object.

wall thickness smaller than that in Figure 9(a). Additionally, as expected from the volume conservation viewpoint (under the condition of a constant extrusion rate and nozzle moving speed), the height of the object in Figure 9(a) is smaller than that in Figure 9(b). In fact, based on the volume conservation, the dimensions (i.e., the wall thickness and height of the object) of the objects extruded with the nozzle height equal to the multi-layer critical nozzle height can be predicted based on the nozzle height, the nozzle diameter, and the critical nozzle height. For example, the object is fabricated with the nozzle height equal to the critical nozzle height (0.65 mm). Thus, there is no nozzle dragging effect or squeezing effect and therefore the wall thickness is expected to be equal to the nozzle diameter (0.8 mm). This is indeed the case as shown in Figure 9(a). Furthermore, since the thickness of each layer is determined by the nozzle height, it is expected that the height of Figure 9(a) (containing 6 layers) would be approximating to 4.5 mm ($6 \times 0.75 \text{ mm}$), which is nearly identical to 3.9 mm measured experimentally. The measured value is slightly lower than the predicted one because of the gravity and shrinkage during drying.

Conclusions

The systematic extrusion based 3D printing studies discussed above clearly show that in order to get universal property of materials and dimension accuracy of the extrudate in DEF processes, extrusion parameters including the nozzle height, the extrusion rate, the nozzle moving speed, and the critical nozzle height should be selected properly. However, favorable effects of the proper selection of these extrusion parameters can be achieved only when the EBC is pseudo-plastic. The latter can be accomplished by adding thickener to the EBC. In this paper, the adopted thickener is alginate. The rheological behavior of EBC (30 wt% alginate) is most suitable for DEF. Once the proper EBC is prepared, extrusion con-

ditions have strong impact on the cross-sectional geometry of the extrudate and the quality of 3D objects fabricated.

An important extrusion parameter, called the critical nozzle height, has been identified in this study. The critical nozzle height is determined by the extrusion rate, nozzle moving speed, and nozzle diameter. When extrusion is carried out with the nozzle height equal to the critical nozzle height, an extruded line with a near 90° contact angle results and when the nozzle height equals to the multi-layer critical nozzle height, the dimensions of the 3D object fabricated are equal to the computer model. Good uniformity of wall thickness and wall uprightness with no wall slumping can be realized. These objects also have good dimensional stability during sintering and their shrinkage is relatively uniform and predictable. When extrusion is carried out with the nozzle height smaller than the critical nozzle height, the forced flow of the EBC will be present and an acute contact angle results. Furthermore, the dimensions of the 3D objects built will not be equal to the computer model. When extrusion is performed with the nozzle height larger than the critical nozzle height, the dimensions of 3D objects fabricated cannot be predicted. Substantial distortion in shape may be present in the objects. As such, extrusion with the nozzle height larger than the critical nozzle height should be avoided.

References

1. J. J. Beaman, J. W. Barlow, D. L. Bourell, R. H. Crawford, H. L. Marcus, and K. P. McAlea, *Solid Freeform Fabrication: A New Direction in Manufacturing*, Kluwer Academic Publishers, Boston, 1997.
2. S. Z. Guo, F. Gosselin, N. Guerin, A. M. Lanouette, M. C. Heuzey, and D. Therriault, *Small*, **9**, 4118 (2013).
3. S. Das, M. Wohlert, J. J. Beaman, and D. L. Bourell, *JOM*, **50**, 17 (1998).
4. J. J. McIntosh, S. C. Danforth, and V. R. Jamalabad, *Proceedings of the Eighth SFF Symposium*, University of Texas, Austin, TX, p 159 (1997).
5. S. W. Park, J. M. Jung, and J. H. Choi, *Polym. Korea*, **41**, 276 (2017).
6. J. S. O, Y. Shin, Y. M. Jeon, B. K. Baek, H. Ahn, and S. Y. Kim, *Polym. Korea*, **41**, 203 (2017).
7. L. J. Gibson, *J. R. Soc. Interface*, **9**, 2749 (2012).
8. D. Dimos, P. Yang, T. J. Garino, M. V. Raymond, and M. A. Rodriguez, *Proceedings of the Eighth SFF Symposium*, University of Texas, Austin, TX, p 33 (1997).
9. S. W. Cho, S. G. Shin, H. J. Kim, S. R. Han, and J. H. Jeong, *Polym. Korea*, **41**, 346 (2017).
10. J. Grau, J. Moon, S. Uhland, M. Cima, and E. Sachs, *Proceedings of the Eighth SFF Symposium*, University of Texas, Austin, TX, p 371 (1997).
11. R. D. Farahani, H. Dalir, V. Le Borgne, L. A. Gautier, M. A. El Khakani, M. Levesque, and D. Therriault, *Nanotechnology*, **23**, 085502 (2012).
12. X. Li, J. Crocker, E. Geiss, L. Shaw, H. Marcus, and T. Cameron, *Proceedings of the 11th SFF Symposium*, University of Texas, Austin, TX, p 159 (2000).
13. L. L. Shaw, X. Li, J. Wang, H. L. Marcus, T. B. Cameron, and C. Kennedy, "Dental restoration through laser densification of dental porcelain powder", in *Rapid Prototyping of Materials*, F. D. S. Marquis and D. L. Bourell, Editors, Warrendale, PA., p 107-116 (2002).
14. J. Wang, X. Li, L. Shaw, H. L. Marcus, and T. B. Cameron, *Proceedings of the 12th SFF Symposium*, University of Texas, Austin, TX, p 546 (2001).
15. R. Clancy, V. Jamalabad, and P. Whalen, *Proceedings of the Eighth SFF Symposium*, University of Texas, Austin, TX, p 185 (1997).
16. M. Agarwala, A. Bandyopadhyay, R. van Weeren, A. Safari, S. C. Danforth, N. A. Langrana, V. Jamalabad, and P. J. Whalen, *Bull. Am. Ceram. Soc.*, **75**, 11 (1996).
17. J. Cesarano III, T. A. Baer, and P. Calvert, *Proceedings of the Eighth SFF Symposium*, University of Texas, Austin, TX, p 25 (1997).
18. J. Davies and J. G. P. Binner, *J. Eur. Ceram. Soc.*, **20**, 1539 (2000).
19. Z. Chen, K. Ikeda, T. Murakami, and T. Takeda, *J. Mater. Sci.*, **35**, 2517 (2000).
20. Y. Du, N. M. Sammes, and G. A. Tompsett, *J. Eur. Ceram. Soc.*, **20**, 959 (2000).
21. D. T. Pham and R. S. Gault, *Int. J. Mach. Tools Manuf.*, **38**, 1257 (1998).
22. R. D. Farahani, H. Dalir, V. Le Borgne, L. A. Gautier, M. A. El Khakani, M. Levesque, and D. Therriault, *Nanotechnology*, **23**, 085502 (2012).
23. S. Ghosh, S. T. Parker, X. Y. Wang, D. L. Kaplan, and J. A. Lewis, *Adv. Funct. Mater.*, **18**, 1883 (2008).
24. S. Z. Guo, F. Gosselin, N. Guerin, A. M. Lanouette, M. C. Heuzey, and D. Therriault, *Small*, **9**, 4118 (2013).
25. R. A. Riggelman, J. F. Douglas, and J. J. de Pablo, *Soft Matter*, **6**, 292 (2010).
26. A. S. Zerda and A. J. Lesser, *J. Appl. Polym. Sci.*, **84**, 302 (2012).
27. J. Benbow and J. Bridgwater, *Paste Flow and Extrusion Oxford Series on Advanced Manufacturing*, Clarendon Press, Oxford, 1993.